

Wind conditions in category 1-3 tropical cyclones can exceed wind turbine design standards

M. Sanchez Gomez¹, J. K. Lundquist^{1,2,3}, G. Deskos², S. R. Arwade⁴, A. T. Myers⁵, J. F. Hajjar⁵

¹Department of Atmospheric and Oceanic Sciences, University of Colorado Boulder, Boulder, Colorado, 80309, United States

²National Wind Technology Center, National Renewable Energy Laboratory, Golden, Colorado, 80401, United States

³Renewable and Sustainable Energy Institute, Boulder, Colorado, 80309, United States

⁴University of Massachusetts Amherst, Amherst, Massachusetts, 01003, United States

⁵Northeastern University, Boston, Massachusetts, 02115, United States

Key Points:

- Turbulence-resolving simulations of tropical cyclones shed light onto the extreme wind conditions that future offshore wind turbines may experience in regions prone to extreme weather events.
- The magnitudes of hub-height wind speeds, vertical shear and wind veer across the turbine rotor layer, may exceed the corresponding extreme wind conditions specified by current international offshore wind design standards.
- Probability distributions of the hub-height mean velocity, velocity profile power-law exponent, velocity variance and yaw misalignment angle, extracted from the present high-fidelity simulation data, support the need to re-visit wind turbine design standards.

Corresponding author: Miguel Sanchez Gomez, misa5952@colorado.edu

Abstract

Offshore wind energy deployment in the US is expected to increase in the years to come, with proposed wind farm sites located in regions with high-risk for tropical cyclones. Yet, the wind turbine design criteria outlined by the International Electrotechnical Commission for extreme events may not account for the severe wind conditions in tropical cyclones, even the weaker storms that are likely to reach mid-Atlantic wind resource areas. To evaluate if current design standards capture the extreme conditions of these storms, we perform idealized large-eddy simulations of five tropical cyclones (two category-1, two category-2, and one category-3 storms) using the Weather Research and Forecasting model. Wind conditions near the eyewall of category-1, category-2 and category-3 storms can exceed current design standards for offshore wind turbines. Hub-height winds can exceed design criteria for Class I and Class T turbines for 50-year recurrence periods. Moreover, wind speed shear across the turbine rotor layer is larger than assumed in design specifications. Vertical variations in wind direction across the turbine rotor layer are also large for tropical cyclones of all intensity levels, suggesting design standards should include veer, which can amplify loads in wind turbines.

1 Introduction

With the US government setting a bold goal of deploying 30 gigawatts (GW) of offshore wind by 2030 (The White House, 2022), future offshore wind energy development will need to be expanded to include U.S. regions that are prone to tropical cyclones, i.e., Gulf of Mexico, Southern U.S. states and Hawaii (Musial et al., 2022). Leasing plans in US hurricane-prone areas are ongoing and large-scale commercial deployment is expected to start before 2030 (Musial et al., 2022). However, the uncertainty associated with the impact of extreme wind conditions under tropical cyclones (1-min sustained winds $>30 \text{ m s}^{-1}$ at 10 m elevation) as well as their recurrence period (between 5 - 16 years) (Neumann, 2010; Keim et al., 2007; Hallowell et al., 2018), which are smaller than the wind farm lifetime (e.g., 25 years), call for a more thorough investigation of the hurricane hazard associated with installing and operating offshore wind turbines in these areas.

The International Electrotechnical Commission (IEC) provides design standards for onshore (61400-1 IEC, 2019a) and offshore (61400-3 IEC, 2019b) wind turbines. The IEC defines wind design classes based on wind speed (Class I, II, III) and turbulence (A+, A, B, C) conditions (IEC, 2019a). As such, Class IA+ turbines may be designed for high-wind conditions with very high turbulence characteristics for deployment in regions with low-risk of extreme weather events. Furthermore, the IEC recently introduced a class T turbine for deployment in regions where tropical cyclones can occur regularly (IEC, 2019a). As such, Class IA+,T wind turbines may be designed for the highest wind conditions and turbulence characteristics. Nonetheless, the Class T wind turbine may not cover wind conditions in all the areas prone to tropical cyclones and therefore a site-specific assessment may be required (IEC, 2019a).

Current design specifications for offshore wind turbines do not account for the complexity in the extreme wind conditions in tropical cyclones. Even though the latest IEC 61400-3 specifications increase the design reference wind speed (U_{ref}) for T class turbines (IEC, 2019b), ultimately strengthening turbine blades and support structures, it may ignore the actual complexity of the extreme wind conditions during a tropical cyclone as well as possible damaging load cases associated with it. Furthermore, wind turbine original equipment manufacturers (OEMs) have yet to deploy class T wind turbines in hurricane-prone regions (e.g., Gulf of Mexico, Southern U.S. states, Hawaii) (Musial et al., 2022) and therefore may have not yet acquired the necessary experience needed to refine their design.

Wind data at turbine heights (below 300 m above the surface) during hurricane events are extremely limited, hindering the understanding of wind conditions that negatively impact wind turbines. Dropsondes released from airplanes can provide valuable data, but do not allow for a temporal or spatial analysis of winds across the rotor layer (Hock & Franklin, 1999; Franklin et al., 2003). Data from meteorological towers could allow for this analysis, however few offshore towers exist (Archer et al., 2016). Given that the most extreme wind conditions in tropical cyclones occur at the radius of maximum winds (i.e., eyewall), a sparse observational network is unlikely to capture extreme conditions during a tropical cyclone. Furthermore, localized observations can underestimate extreme wind conditions, even if experiencing a direct hit, due to under-sampling (Nolan et al., 2014). Doppler radars, like the Doppler On Wheels (DOW), are able to capture the spatial distribution of winds in hurricanes (Marks & Houze, 1984; Wurman & Winslow, 1998; Wurman & Kosiba, 2018). DOW observations have already linked tornado-scale vortices and mesovortices to increased surface winds in tropical cyclones (Wurman & Kosiba, 2018). Even though Doppler radars can capture flow characteristics at varying heights, the high-temporal/spatial resolution measurements required to quantify turbulence at turbine heights are still lacking.

Scale-resolving, large-eddy simulations (LES) can provide simulated wind fields that capture the turbulence structures across multiple atmospheric length scales and provide high-fidelity, tropical cyclone boundary layer solutions. LES capture the dominant physical mechanisms that drive tropical cyclones. For instance, LES of Hurricane Harvey suggest turbulence is mainly driven by roll vortices (Li et al., 2021), which are not captured in analytical turbulence models. High-fidelity simulations can also provide insight into the spatial complexity of storms. Stern et al. (2021) reports wind gusts exceeding 70 m s^{-1} occur consistently over a small radial region for high-intensity storms, but are rare outside this region. Similarly, Ren et al. (2022) show strong localized updrafts occur in intense hurricanes, which can enhance turbulence.

LES of tropical cyclones can be used to inform wind turbine design standards. Previous idealized LES of a category-5 storm show current design specifications underestimate gusts near the eyewall (Worsnop, Lundquist, et al., 2017). Turbulence spectral coherence within the tropical cyclone boundary layer can also be higher than the one proposed by the IEC standards and employed by various spectral models (Worsnop, Bryan, et al., 2017). Similarly, turbulence in the boundary layer of tropical cyclones displays higher energy at high frequencies compared to some of the IEC-recommended spectral models (Worsnop, Bryan, et al., 2017).

Wind conditions relevant for wind turbine design have not been studied in depth for low-intensity tropical cyclones. Previous work focused on understanding wind conditions for Category-5 storms, where 1-min sustained winds exceed 70 m s^{-1} (Worsnop, Lundquist, et al., 2017; Worsnop, Bryan, et al., 2017). Category-5 storms have a higher destructive potential than lower intensity tropical cyclones. However, category-1 and category-2 storms are more likely to occur in the Gulf of Mexico and East Coast of the US compared to category-5 storms (Neumann, 2010; Keim et al., 2007; Hallowell et al., 2018).

Here, we use LES of five tropical cyclones (two category-1, two category-2 and one category-3) to evaluate current design standards for offshore wind turbines and inform future development. We compare mean and turbulence wind conditions from five tropical cyclones of different sizes and intensity levels to the IEC design specifications. Storms of different size and similar intensity can provide insight into the differences in the spatial distribution of extreme winds in tropical cyclones. Furthermore, we recommend additional atmospheric conditions that should be taken into account in wind turbine design criteria.

This paper is structured as follows. Section 2 describes the simulation methodology. In section 3, we present the tropical cyclones' evolution throughout our simulations.

The intensity of each tropical cyclone is reported in section 4. Section 5 compares wind conditions in our simulations with current design specifications for offshore wind turbines. Lastly, we summarize our findings and suggest future research in section 6.

2 Simulation setup

We perform LES of five tropical cyclones using the Weather Research and Forecasting (WRF) model v4.1.5 (Skamarock et al., 2019) with a five domain (d01-d05), one-way nesting setup. The first three domains, d01-d03, with horizontal resolutions of $\Delta x = 13.5$ km, 4.5 km and 1.5 km, use a planetary boundary layer (PBL) scheme for turbulence closure. The number of grid points in the x - and y -directions for each of the mesoscale domains are 300×300 , 320×320 and 320×320 , respectively. We simulate five tropical cyclones with different intensity levels by varying the surface temperature, T_s . Because warmer surface temperatures increase the size and intensity of the tropical cyclone, we use different domain configurations for the LES domains (Table 1). All domains use 109 vertical grid points, having the lowest unstaggered vertical level at 10 m above the surface. The grid refinement ratio between d03 and d04 is larger than the commonly utilized factor of 3, similar to Muñoz-Esparza et al. (2017), to avoid unrealistic modeling at resolutions within the *terra incognita* regime (Wyngaard, 2004), where neither PBL schemes nor LES closures are appropriate, and to avoid having spurious structures contaminant the finer domains (Mazzaro et al., 2017).

Table 1. Simulation setup, including surface temperature T_s , tropical cyclone category, radius of maximum winds R , horizontal resolution $\Delta x, \Delta y$, and number of grid points (n_x, n_y, n_z).

T_s [$^{\circ}\text{C}$]	Category	R [km]	Domain	$\Delta x, \Delta y$ [m]	n_x, n_y, n_z
26	1	13.8	d04	166.67	(658, 658, 109)
			d05	55.55	(1201, 1201, 109)
28	1	21.3	d04	166.67	(658, 658, 109)
			d05	55.55	(1201, 1201, 109)
30	2	20.3	d04	166.67	(757, 757, 109)
			d05	55.55	(1303, 1303, 109)
32	2	27.1	d04	166.67	(757, 757, 109)
			d05	55.55	(1303, 1303, 109)
34	3	33.6	d04	166.67	(865, 865, 109)
			d05	55.55	(1603, 1603, 109)

We simulate five distinct tropical cyclones by varying surface forcing and the initial potential temperature and water vapor mixing ratio profiles. Similar to Ren et al. (2020, 2022), we vary the intensity of each storm by modifying surface temperature between 26 $^{\circ}\text{C}$ and 34 $^{\circ}\text{C}$. The temperature and water vapor mixing ratio profiles from Jordan (1958) are used to initialize our simulations. The potential temperature and water vapor mixing ratio profiles are modified as $\theta(z) = \theta_0 + (T_s - 28)$ and $q_v(z) = q_{v0}(1 \pm 0.07^{T_s - 28})$, where the sign of $0.07^{T_s - 28}$ is positive if $T_s > 28$ $^{\circ}\text{C}$ and negative otherwise, to accommodate differences in surface forcing (Ren et al., 2020, 2022). The velocity field is initialized with a tropical cyclone-like axisymmetric vortex with a maximum wind speed of 15 m s^{-1} , radius of maximum wind of 82.5 km, and radius of zero wind of 412.5 km (Rotunno & Emanuel, 1987), as in previous studies (Rotunno et al., 2009; Ren et al., 2020, 2022).

Cloud physics in all domains are parameterized using the WRF Single-Moment 6-Class cloud physics (S. Hong & Lim, 2006). The mesoscale domains (d01-d03) use the YSU planetary boundary layer scheme to parameterize turbulence mixing (S.-Y. Hong et al., 2006). The LES domains (d04-d05) in the 26 °C to 32 °C simulations use the TKE-1.5 order closure to parameterize subgrid-scale (SGS) fluxes of momentum and heat (Moeng et al., 2007). We found surface winds are sensitive to SGS model: the nonlinear backscatter and anisotropy (NBA) SGS model produced faster winds at 10 m compared to the TKE-1.5 order closure for the 34 °C simulation (not shown). Therefore, the LES domains in the 34 °C simulation use the NBA model with turbulence kinetic energy (TKE)-based stress terms (Kosović, 1997; Mirocha et al., 2010) to simulate the highest-intensity storm. Surface boundary conditions are specified using Monin-Obukhov similarity theory (Jiménez et al., 2012) for 10 m winds slower than 25 m s⁻¹. All domains use an alternative formulation of the surface heat and momentum exchange coefficients for 10 m winds faster than 25 m s⁻¹, appropriate for strong winds in ocean environments (Donelan, 2004). The drag coefficient is capped at 0.0024, while the heat exchange coefficient increases linearly with the thermal length z_{0q} (Dudhia et al., 2008).

We evaluate the spatial and temporal evolution of wind statistics using high-frequency output. The instantaneous velocity components, pressure and potential temperature are output at every time step at multiple radial ($r/R = [0.8, 1.2]$ in 0.06 r/R increments) and azimuthal ($\alpha = [0^\circ, 90^\circ]$ in 10° increments) locations in our LES domains. The high-frequency output for domain d04 is at ~6 Hz and for d05 is at ~18 Hz. Furthermore, the three-dimensional velocity, temperature and pressure fields for the entire domain are output every 5 min.

3 Tropical cyclone development

These incipient tropical storms evolve into tropical cyclones of different intensity levels as surface temperatures change. The evolution of the storm varies for each tropical cyclone and each domain. Due to the increased computational cost of the LES domains, we first develop a tropical cyclone in the mesoscale domains and then initialize the turbulence-resolving domains as in Ren et al. (2022, 2020).

We evaluate spin-up of the mesoscale domains based on the maximum instantaneous wind speed at the surface. Domains d01-d02 are initialized simultaneously and reach a quasi-steady state after approximately four days (Figure 1). At this point, domain d03 is initialized. Maximum instantaneous wind speeds do not vary significantly between domains d02 and d03. Nonetheless, domain d03 runs for three additional days so that it reaches its own resolved steady state.

In general, warmer surface temperatures result in faster surface winds in the mesoscale domains (Figure 1). Even though all tropical cyclones are initialized with the same velocity field, maximum instantaneous wind speed for domain d03 at 10 m above the surface is 45.5 m s⁻¹, 58.01 m s⁻¹, 72.87 m s⁻¹, 76.71 m s⁻¹ and 84.87 m s⁻¹ for the 26 °C, 28 °C, 30 °C, 32 °C and 34 °C simulations, respectively.

We evaluate spin-up of the LES domains using turbulence evolution in the boundary layer. Due to the strong winds, turbulence propagates rapidly across all resolvable scales in the LES domains. For domain d04, turbulence spectra at the surface for a radial location r far away from the tropical cyclone eyewall R , ($\hat{r} = r/R = 1.8$), converge 1 h after initialization (Figure 2a). However, wind speed at the surface takes longer than turbulence to stabilize (Figure 3). Maximum instantaneous surface winds stabilize 4 h after initialization for the $T_s = 26$ °C to 32 °C simulations, and 2 h after initialization for the $T_s = 34$ °C simulation. For domain d05, turbulence spectra away from the eyewall converge 5 min after initialization (Figure 2b). Turbulence spectra for d04 and d05 levels off for $k > 1/8\Delta x$ because the effective grid resolution of WRF is $7 - 8\Delta x$

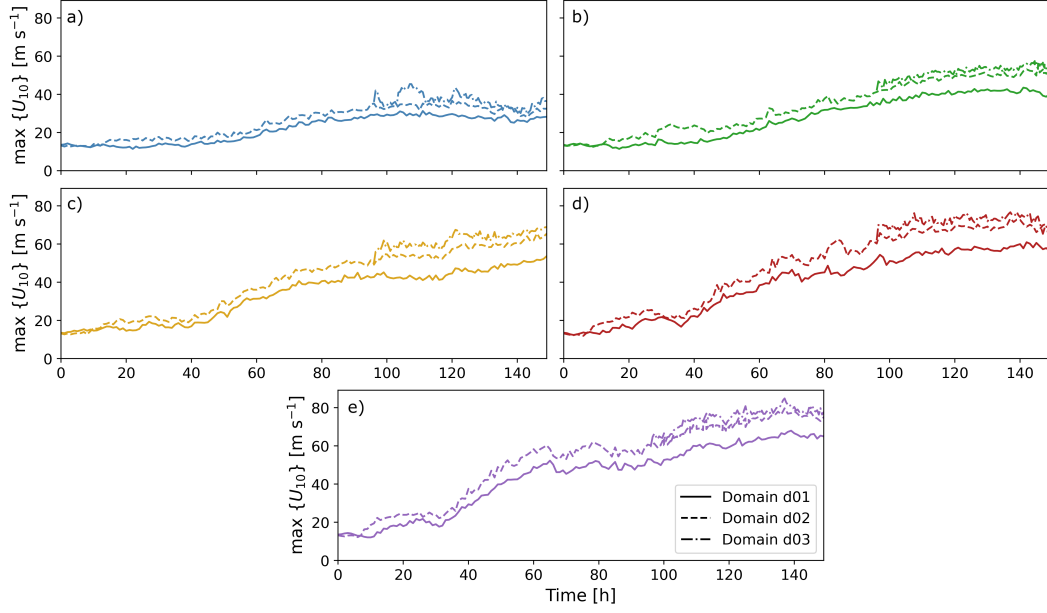


Figure 1. Temporal evolution of maximum instantaneous wind speed at 10 m above the surface in each mesoscale domain for the a) 26 °C, b) 28 °C, c) 30 °C, d) 32 °C, and e) 34 °C tropical cyclone simulations.

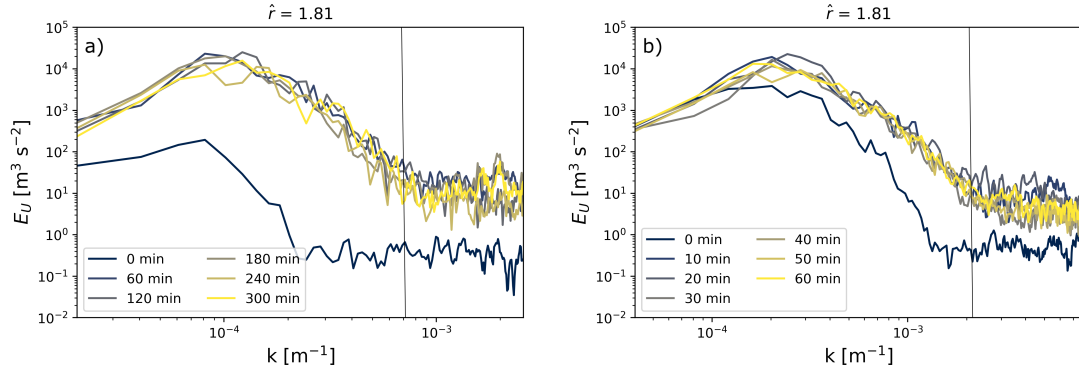


Figure 2. Turbulence spectra of the streamwise velocity at a radial location, $r = 1.8R$, for domain d04 (a) and domain d05 (b) at 10 m above the surface for the $T_s = 26$ °C simulation. Turbulence spectra are color coded for minutes since initialization for each domain. The vertical black lines represent the effective resolution of WRF ($7 - 8\Delta x$) (Skamarock, 2004).

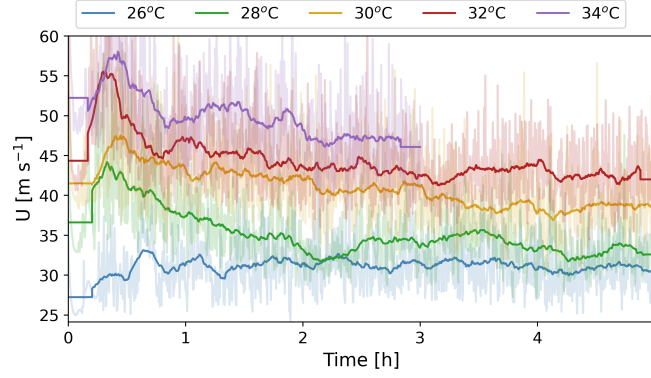


Figure 3. Time series of maximum streamwise wind speed at the surface (10 m) for domain d04. The light colored lines represent instantaneous maximum wind speed at every time step in the domain. The dark colored lines represent the 10-min moving average.

(Skamarock, 2004). Note that we only present turbulence evolution for the lowest-intensity tropical cyclone because turbulence spin-up is faster in the other cases. The high-resolution LES domain for the $T_s = 26^\circ\text{C}$ to 32°C simulations is run for 65 min, from which the first 5 min are ignored due to turbulence spin-up. Domain d05 in the $T_s = 34^\circ\text{C}$ tropical cyclone is run for only 50 min due to increased computational cost.

Just as winds are faster with increasing surface temperatures, the size of the tropical cyclone also increases (Figure 4) with increasing surface temperatures in these simulations, as in (Ren et al., 2020). The radius of maximum wind speed at 10 m above the surface, R , is on average at 13.8 km, 21.3 km, 20.3 km, 27.1 km and 33.6 km from the center for the 26°C to 34°C simulations, respectively. Throughout the simulation period, surface winds at the eyewall are on average 25 m s^{-1} , 27 m s^{-1} , 35 m s^{-1} , 36 m s^{-1} and 39 m s^{-1} for the $T_s = 26^\circ\text{C}$ to 34°C tropical cyclones, respectively. We evaluate wind statistics at radial locations near the eyewall ($\hat{r} = r/R = [0.8, 1.2]$) to quantify the extreme wind conditions that occur in tropical cyclones. Note that for largest storms (i.e., $T_s = 32^\circ\text{C}$ and 34°C) $\hat{r} = [0.8, 1.2]$ spans a radial distance of more than 10 km.

4 Tropical cyclone intensity

Two category-1, two category-2 and one category-3 tropical cyclones are simulated by increasing surface temperature T_s from 26°C to 34°C (Figure 5). We define the category of each tropical cyclone using the Saffir-Simpson wind scale (National Hurricane Center, 2021), commonly used to determine storm intensity and property damage. Maximum 1-min sustained winds at 10 meters above the surface in domain d05 are on average 35.04 m s^{-1} , 38.08 m s^{-1} , 47.26 m s^{-1} , 46.19 m s^{-1} and 50.05 m s^{-1} for the 26°C , 28°C , 30°C , 32°C and 34°C simulations, respectively (Figure 5). As a result, tropical cyclones with $T_s = 26^\circ\text{C}$ and 28°C are on average category-1, $T_s = 30^\circ\text{C}$ and 32°C are on average category-2, and $T_s = 34^\circ\text{C}$ is on average a category-3. Because wind speed changes with grid resolution, we define the intensity of each storm using 1-min averaged wind speed in domain d05 only. Furthermore, the remaining analysis only considers wind conditions in the highest resolution domain.

From hereon, we refer to each tropical cyclone based on its intensity level (category-1, 2 or 3) and eyewall radius (R). As such, the tropical cyclone forced with $T_s = 26^\circ\text{C}$ is a category-1 storm with radius of maximum winds $R = 13.8\text{ km}$, and so on, as listed in Table 1.

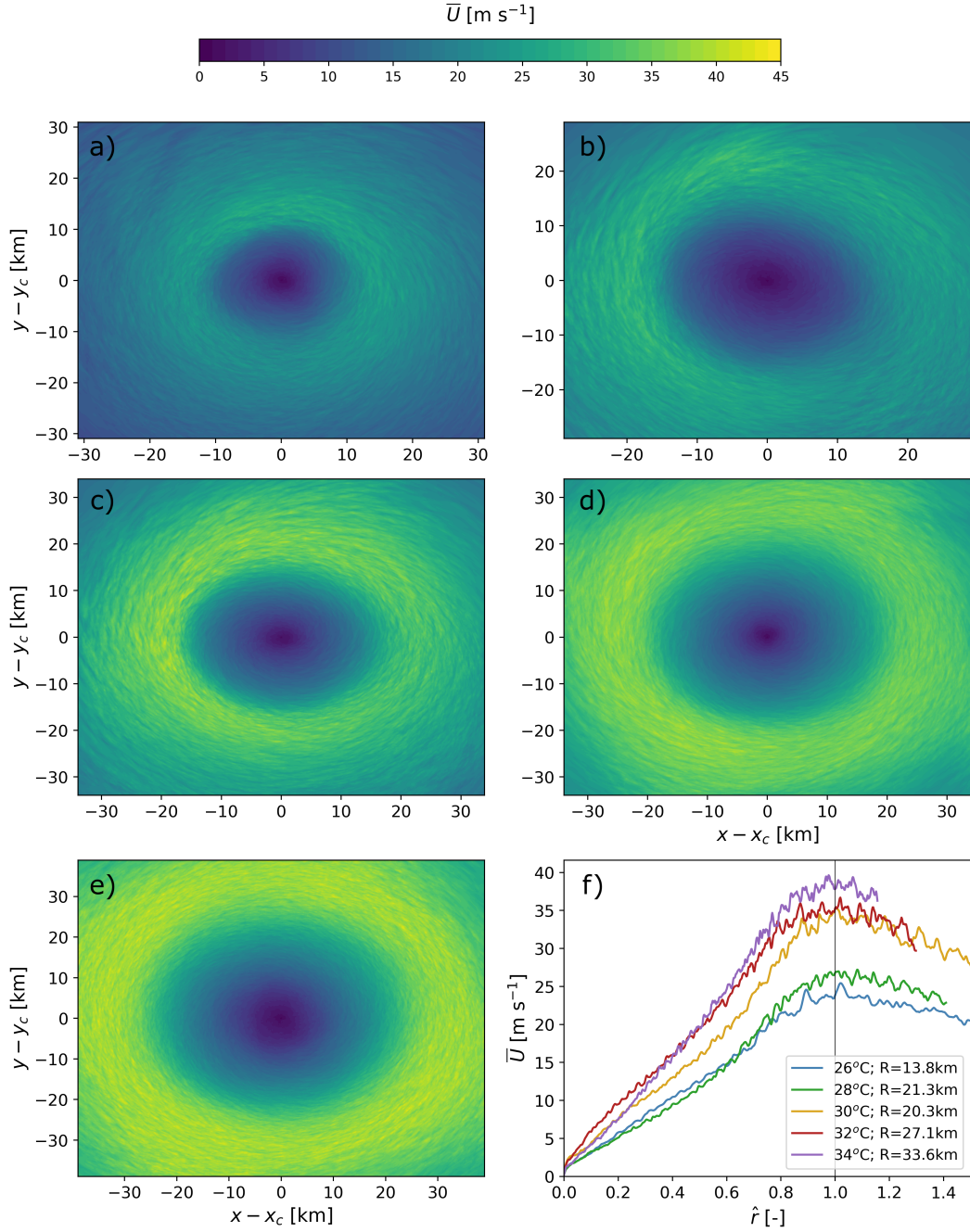


Figure 4. Time-averaged horizontal wind speed at 10 m above the surface for the a) 26 °C, b) 28 °C, c) 30 °C, d) 32 °C, and e) 34 °C tropical cyclone simulations. Panel (f) shows the radial distribution of horizontal wind speed for all tropical cyclones. The x -axis in panel (f) represents the normalized radial location $\hat{r} = r/R$. The velocity fields are averaged over the 50- or 60-min simulation time period.

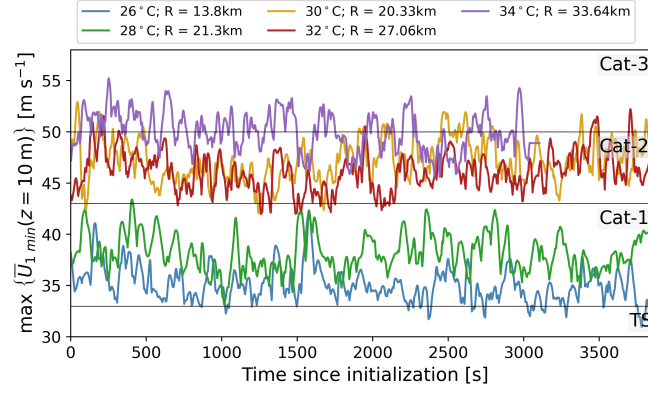


Figure 5. Time series of maximum 1-min averaged horizontal wind speed at 10 m above the surface for each tropical cyclone. For reference, the horizontal black lines illustrate the wind speed thresholds for the Tropical Storm (TS), Category-1 (Cat-1), Category-2 (Cat-2) and Category-3 (Cat-3) denominations in the Saffir-Simpson scale.

5 Wind conditions relevant for offshore turbine design

The IEC standards (IEC, 2019a, 2019b) specify atmospheric conditions for extreme events, such as tropical cyclones, for offshore wind turbine design. Because hub-height wind speeds in tropical cyclones exceed the operational cut-out wind speed, wind turbines are expected to be parked during a tropical cyclone and their rotors to be in a standstill or idling condition. Design load cases (DLC) during parked design situations include the combination of extreme wind and wave conditions (DLC 6.1-6.4), we only consider extreme wind conditions here. In particular, extreme wind models recommended by the IEC standards include 10-min and 3-sec analysis using the reference wind speed with a recurrence period of 50 years, and the standard deviation of the horizontal wind as a proxy for turbulence (IEC, 2019a). Furthermore, yaw misalignment is also considered as a loads amplifying factor with a maximum, mean yaw misalignment of $\pm 20^\circ$ or $\pm 8^\circ$, depending on the extreme wind model. In both cases, an active yaw system is assumed to be in place and the absence of slippage is also assured. Finally, Annex I of the IEC 61400–3 standards specify two additional DLCs (i.e. I.1 and I.2) specifically for areas prone to tropical cyclones, which allow for an increase in the design return period (from 50 years to 500 years). For DLC I.1, 10-min averaged winds with a 500-year return period should be estimated using the local climatology of the site. For DLC I.2, the return period for winds should be selected such that the joint event of loss of yaw power and controls during the extreme environmental conditions is 500 years.

We contrast wind conditions from the IEC design standards for offshore wind turbines against the conditions calculated by the LES of tropical cyclones. In this way, we compare 10-min and 3-sec winds in the turbine rotor layer with a 50-year recurrence period from the IEC 61400–3 standard with 10-min and 3-sec averaged winds from each tropical cyclone simulation. We also compare turbulence in the tropical cyclone boundary layer against the assumed turbulence from the IEC standards. Furthermore, we evaluate the temporal and spatial evolution of wind direction in the turbine rotor layer. For reference, we consider the NREL 5MW wind turbine for offshore development with hub height at 90 m above the surface and rotor diameter D of 126 m (Jonkman et al., 2009).

5.1 Extreme wind models

Design loads are evaluated using a variety of wind models with a reference wind speed. For parked conditions, such as during a tropical cyclone event, design loads are evaluated using the steady extreme wind speed model and the turbulent extreme wind speed model. The steady extreme wind speed model provides guidance on 3-sec averaged winds in the turbine rotor layer with 50-year (U_{e50}) recurrence period (Equation 1). The turbulent extreme wind speed model provides guidance on 10-min averaged winds in the turbine rotor layer with 50-year (U_{50}) recurrence period (Equation 2). The latest IEC standard for offshore wind turbines (IEC, 2019b) requires the use of the turbulent extreme wind speed model for DLC 6.1-6.4; conversely, either extreme wind speed model can be used for onshore wind turbine design (IEC, 2019a). Herein, we contrast both models against wind conditions in tropical cyclones. For the IEC Class IA+ turbine, the most robust turbine class in the IEC standards for deployment in regions with low-risk for tropical cyclones, the reference wind speed (U_{ref}) and turbulence intensity (I_{ref}) are 50 m s^{-1} and 0.18, respectively. For the IEC Class IA+,T turbine (Class T from hereon), the most robust turbine class in the IEC standards for deployment in regions where tropical cyclones can occur, the reference wind speed ($U_{\text{ref,T}}$) and turbulence intensity are 57 m s^{-1} and 0.18, respectively.

$$U_{e50}(z) = 1.4 U_{\text{ref}} \left(\frac{z}{z_h} \right)^{0.11} \quad (1)$$

$$U_{50}(z) = U_{\text{ref}} \left(\frac{z}{z_h} \right)^{0.11} \quad (2)$$

Hub-height wind gusts in tropical cyclones rarely exceed design standards for the Class I and Class T turbines (Figure 6a). The black (grey) vertical line in Figure 6a denote design specifications for the Class I (Class T) turbine for 50 year return periods. Wind gusts are larger than design criteria for the Class I turbine less than 10% of the time for category-2 and category-3 storms. For Class T turbines, wind gusts exceed design specifications less than 1% of the time in category-2 and category-3 storms. Wind gusts in category-1 tropical cyclones do not exceed 50-year design criteria for Class I and Class T turbines.

Mean (10-min) hub-height winds in category-2,3 tropical cyclones typically exceed design standards for Class I turbines (Figure 6b). Over the simulated time period, 10-min averaged hub-height winds near the eyewall can exceed 50-year Class I turbine design standards at least 85% of the time in category-2 storms. Mean hub-height winds

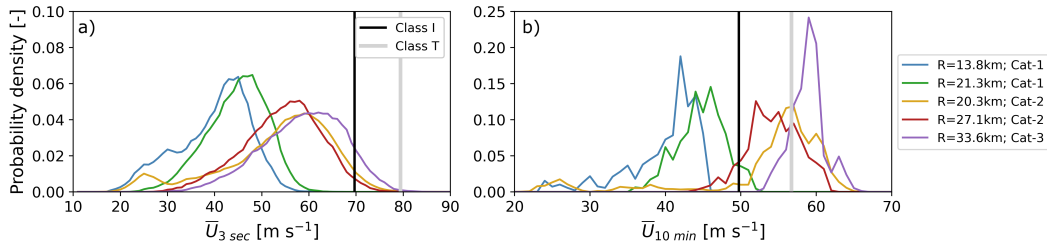


Figure 6. Probability density of 3-sec (a) and 10-min (b) averaged winds at hub height for radial locations between $\hat{r} = [0.8, 1.2]$. The vertical black (grey) lines illustrate the extreme winds for the Class I (Class T) turbine in the IEC standards with a 50-year recurrence period for the steady (a) and turbulent (b) extreme wind speed models.

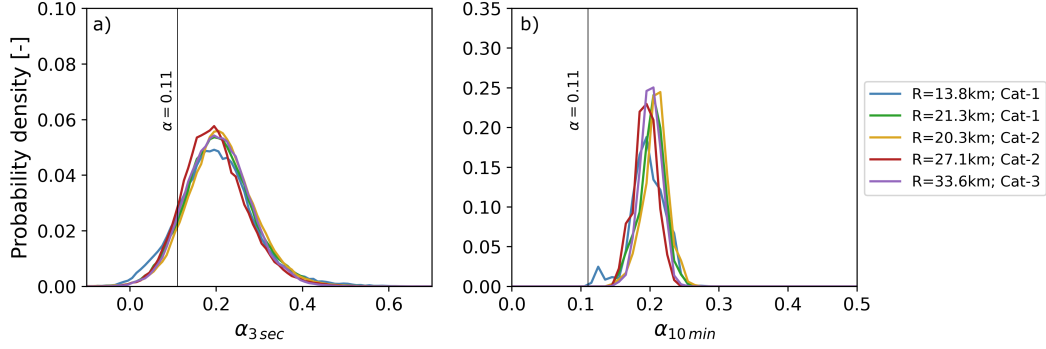


Figure 7. Probability density of the power-law exponent fit to the 3-sec (a) and 10-min (b) averaged wind profiles for radial locations between $\hat{r} = [0.8, 1.2]$. The vertical black line illustrates the power-law exponent from the IEC standards $\alpha = 0.11$.

near the eyewall of the category-3 storm always exceed design criteria for Class I turbines. Mean winds in the category-1 tropical cyclones are faster than design standards for the Class I turbine less than 10% of the time.

Hub-height winds averaged over 10-min in category-2,3 tropical cyclones sometimes exceed Class T turbine design standards (Figure 6b). Winds (10-min averaged) near the eyewall of the category-2 storms exceed design criteria for Class T turbines at least 28% of the time. In the highest intensity storm, mean hub-height winds exceed design criteria 86% of the time. Mean winds at hub height in the category-1 tropical cyclones do not exceed 50-year design criteria for the Class T turbine.

Current standards underestimate the extreme vertical shear of the horizontal wind that can occur in the turbine rotor layer during extreme events (Figure 7). Instead, the steady and turbulent extreme wind models (Equations 1 and 2) prescribed in the standards suggest a power-law wind profile during extreme events with an exponent $\alpha = 0.11$. However, wind profiles for the category-1, category-2 and category-3 tropical cyclones consistently display larger shear (Figure 7). More than 85% of 3-sec averaged wind profiles evidence larger shear than design specifications for all tropical cyclones. Moreover, virtually all 10-min averaged wind profiles display shear larger than $\alpha = 0.11$. The mean power law exponent for both 3-sec and 10-min averaged wind profiles near the eyewall is about 0.20 for all tropical cyclones. In addition, shear for 3-sec (10-min) averaged winds exceeds $\alpha = 0.32$ (0.22) at least 5% of the time for all tropical cyclones.

The extreme wind speed models from the IEC standards fail to account for complex wind profiles, which typically occur over short time periods (Figure 8). Figure 8 shows the wind profile of the median hub-height wind speed for a 3-sec and 10-min averaging periods. Wind profiles representing 3-sec averaged conditions can often display local maxima within the rotor layer, which could impact loads (Figure 8f-j). This variability is also evidenced in the larger spread of the power law exponent for the 3-sec winds compared to the 10-min averaged winds (Figure 7). Even though the 10-min averaged wind profiles do not typically display a local maxima within the rotor layer, wind speed in the upper turbine rotor layer can exceed 50-year design standards for Class I and Class T turbines due to larger-than-expected wind shear (Figure 8a-e).

5.2 Turbulence model

IEC wind turbine design specifications recommend the Mann uniform shear model (Mann, 1994) or the Kaimal spectral model (Kaimal et al., 1972) for design load calcu-

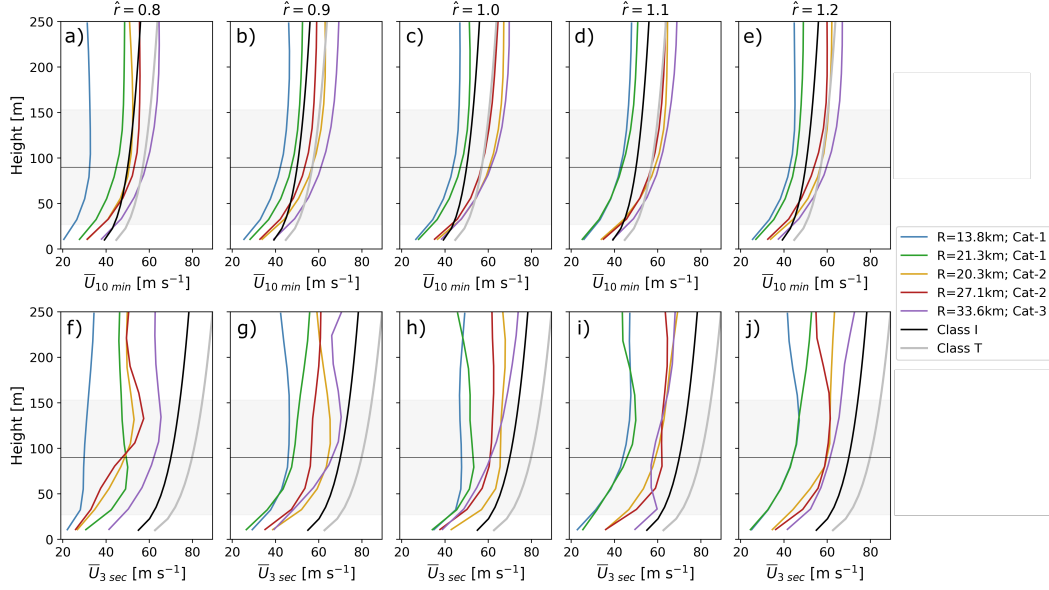


Figure 8. Wind profiles of the median hub-height wind speed for a 10-min (a-e) and 3-sec (f-j) averaging periods. Wind speed profiles are shown at multiple radial locations: $\hat{r} = 0.8$ (a,f), $\hat{r} = 0.9$ (b,g), $\hat{r} = 1.0$ (c,h), $\hat{r} = 1.1$ (d,i), and $\hat{r} = 1.2$ (e,j). The solid black (grey) lines in each panel represent the wind profile for the Class I (Class T) turbine for the turbulent (a-e) and steady (f-j) extreme wind speed models in the IEC standards with a 50-year recurrence period. The grey shaded area in each panel represents the turbine rotor layer. The horizontal black line illustrates hub height.

lations (IEC, 2019a). Even though these models may not represent the spectral energy in the tropical cyclone boundary layer (Worsnop, Bryan, et al., 2017), we will focus on the total energy contained over all frequencies, namely the variance of the horizontal velocity. An input to the Mann and Kaimal models is the standard deviation of the streamwise velocity σ_1 , commonly estimated using the normal turbulence model (Equation 3). As recommended in the IEC standards (IEC, 2019a, 2019b), the standard deviation of the streamwise wind is estimated using a 10-min moving average.

$$\begin{aligned} \sigma_1 &= I_{\text{ref}}(0.75 U_{\text{hub}} + b) \\ U_{\text{hub}} &= 0.7 U_{\text{ref}} \\ b &= 5.6 \text{ m s}^{-1} \end{aligned} \quad (3)$$

The normal turbulence model underestimates variability in the tropical cyclone boundary layer, especially for the high-intensity tropical cyclones (Figure 9). The standard deviation of the streamwise wind at hub height is frequently larger than the normal turbulence model for the Class I and Class T turbines. For the category-1 storms, σ_1 exceeds the normal turbulence model 23% (16%) of the time for the Class I (Class T) turbine. For the category-2 storms, σ_1 exceeds the normal turbulence model 38% (30%) of the time for the Class I (Class T) turbine. Finally, for the category-3 storm, σ_1 exceeds the normal turbulence model 44% (37%) of the time for the Class I (Class T) turbine. Furthermore, the 95th percentile of σ_1 in the eyewall vicinity is greater than 10 m s^{-1} , 13 m s^{-1} and 15 m s^{-1} for the category-1, category-2 and category-3 tropical cyclones,

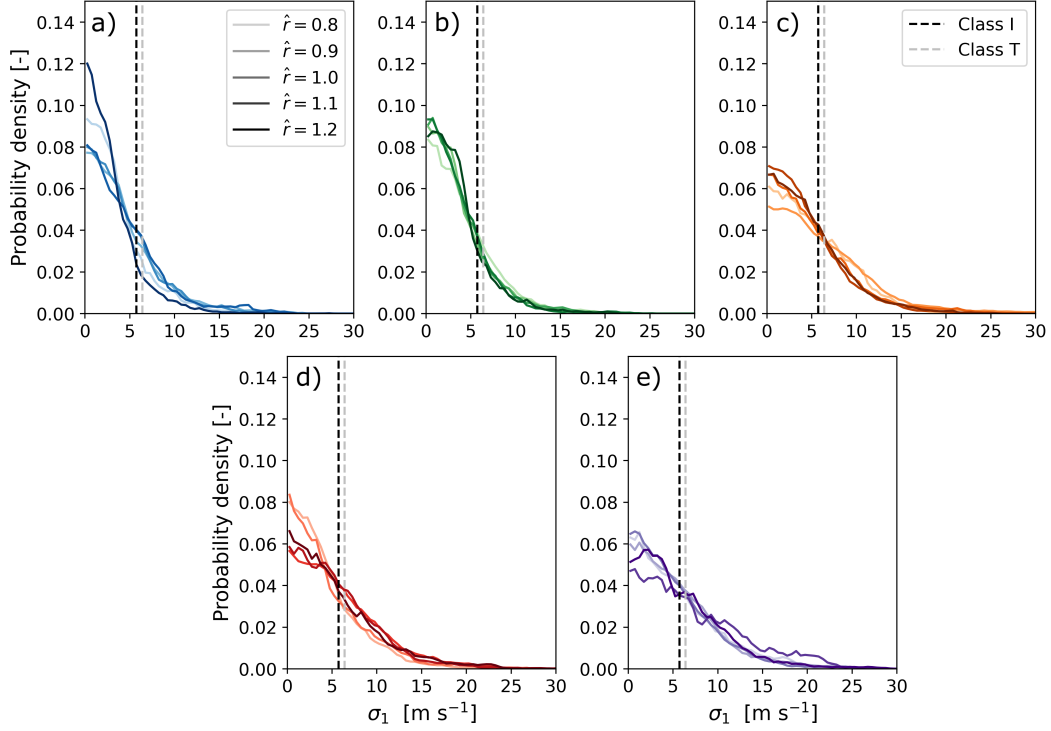


Figure 9. Probability density of the standard deviation of the streamwise velocity for the category-1 $R = 13.8$ km (a), category-1 $R = 21.3$ km (b), category-2 $R = 20$ km (c), category-2 $R = 27.1$ km (d), and category-3 $R = 33.6$ km (e) tropical cyclones. Probability distributions are color-coded for radial locations between $\hat{r} = [0.8, 1.2]$. The dashed vertical black (grey) line illustrates the standard deviation of the streamwise velocity from the normal turbulence model for the Class I (Class T) turbine.

respectively. Thus, the normal turbulence model does not represent the extreme wind variability that can occur in the tropical cyclone boundary layer.

5.3 Yaw misalignment

The design specifications the IEC 61400–3 requires parked turbines to consider wind direction changes for loads analysis. Yaw misalignment is the horizontal wind direction deviation from the wind turbine rotor axis. The standard dictates that a $\pm 20^\circ$ and a $\pm 8^\circ$ yaw misalignment should be considered when estimating loads using the steady and the turbulent extreme wind model, respectively.

Hub-height winds change direction rapidly near the tropical cyclone eyewall (Figure 10). Rapid wind direction changes over 10-sec intervals occasionally exceed 8° . On average for all tropical cyclones, 10-sec changes in hub-height wind direction exceed 8° 17% of the time. However, our simulations suggest winds rarely change direction by more than 20° over a 10-sec time period. Throughout the simulation period, winds change direction by more than 20° over a 10-sec period at most 3% of the time, and on average for all tropical cyclones only 1% of the time. While our results differ from the large shifts in wind direction reported by Worsnop, Lundquist, et al. (2017), we are simulating different storms: they simulate a category-5 tropical cyclone whereas our highest-intensity

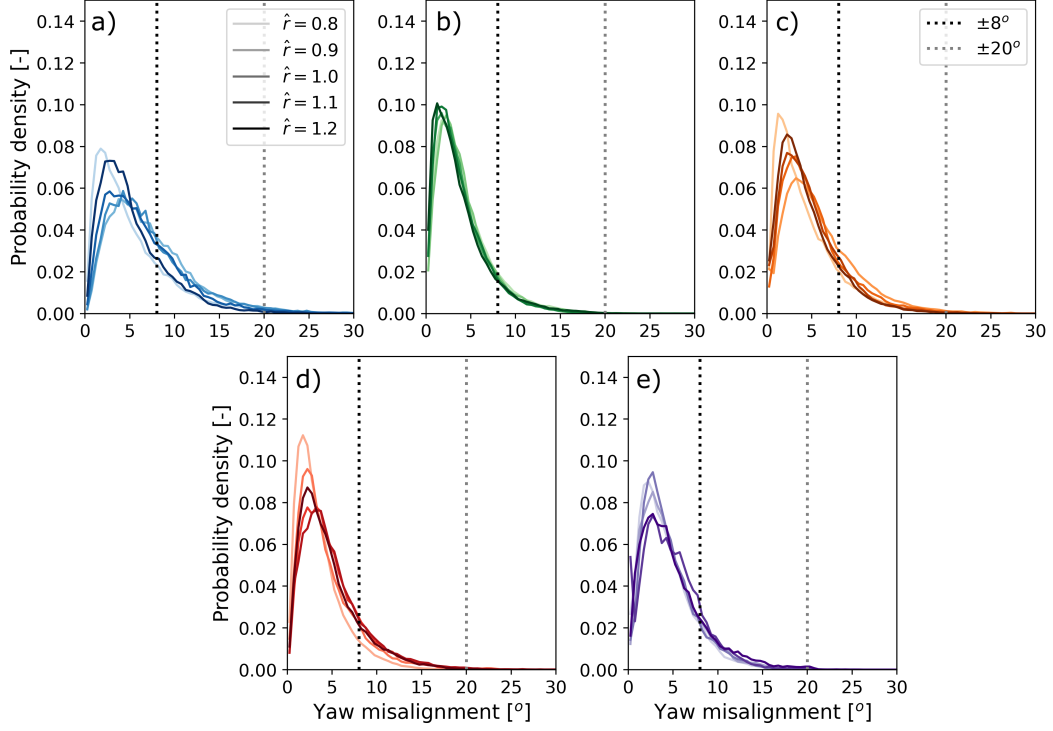


Figure 10. Probability density of yaw misalignment for the category-1 $R = 13.8$ km (a), category-1 $R = 21.3$ km (b), category-2 $R = 20$ km (c), category-2 $R = 27.1$ km (d), and category-3 $R = 33.6$ km (e) tropical cyclones. Probability distributions are color-coded for radial locations between $\hat{r} = [0.8, 1.2]$. The dotted vertical black (grey) line illustrates the $\pm 8^\circ$ ($\pm 20^\circ$) misalignment from the IEC standards for reference.

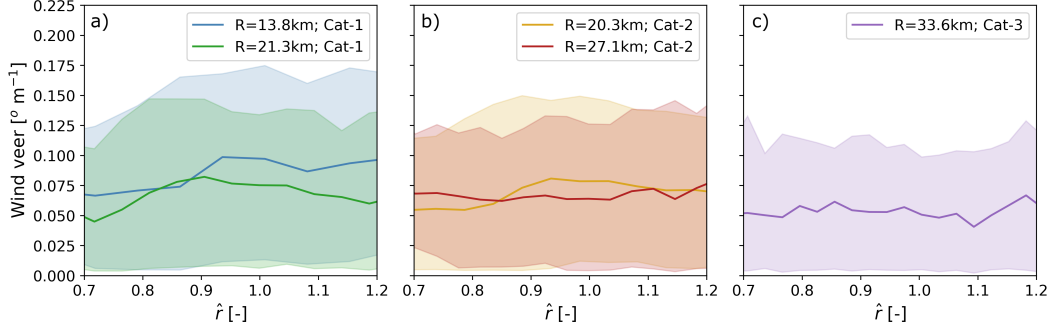


Figure 11. Radial distribution of median wind veer over the turbine rotor layer for the category-1 (a), category-2 (b), and category-3 (c) tropical cyclones. The colored shaded regions on each plot represent the 95% confidence intervals.

storm is category 3. Furthermore, they only report the maximum yaw misalignment at each radial location (Worsnop, Lundquist, et al., 2017).

5.4 Wind veer

Just as wind speed varies with height, wind direction also changes in the vertical direction. This vertical variation in wind direction is called wind veer. Wind veer is not considered in current design specifications, even though it typically occurs in the atmospheric boundary layer onshore (Vanderwende et al., 2015) and offshore (Bodini et al., 2019), and can impact turbine performance (Sanchez Gomez & Lundquist, 2020; Bardal et al., 2015; Gao et al., 2021) and loads (Churchfield & Sirnivas, 2018; Robertson et al., 2019; Kapoor et al., 2020). Veer is defined as the shortest rotational path between the wind vectors at the bottom and top of the turbine rotor layer, here normalized over the turbine rotor diameter D . We estimate wind veer using the difference in 10-sec averaged wind direction at the top ($z = 153$ m) and bottom ($z = 27$ m) of the turbine rotor layer.

Wind veer remains largely unchanged along the radius of the tropical cyclone close to the eyewall for all storm intensities (Figure 11). For the category-1 storms, median wind veer close to the eyewall is on average 0.083 and $0.068^\circ \text{m}^{-1}$. For the category-2 storms, median wind veer is on average 0.069 and $0.066^\circ \text{m}^{-1}$. For the category-3 storm, median wind veer is on average $0.053^\circ \text{m}^{-1}$. The weaker tropical cyclones evidence larger variability in wind veer than the high-intensity tropical cyclones, as shown by the 95% confidence intervals at each radial location (Figure 11). This increased variability is likely due to larger eddies forming in the high-intensity tropical cyclones, resulting in coherent structures that span the turbine rotor layer.

6 Conclusions

Wind conditions in tropical cyclones relevant for wind turbine design are not well understood and data are scarce. As a result, design standards for offshore wind turbines may misrepresent extreme conditions in tropical cyclones. We perform idealized LES of five storms to evaluate current turbine design standards. We evaluate mean and turbulence wind statistics in the tropical cyclone boundary layer and compare them with IEC design specifications. We find likely wind conditions near the eyewall of category-1, category-2 and category-3 storms can exceed current design standard recommendations.

In particular, mean (10-min) hub-height wind speed in the eyewall vicinity is frequently faster than expected in offshore design standards, especially for category-2 and

category-3 tropical cyclones (Figure 6b). Average 10-min winds in category-2 and category-3 cyclones exceed 50-year design specifications for both Class I and Class T turbines at least one third of the time. Category-1 storms typically do not exceed 50-year design criteria. The IEC 61400–3 standard requires the use of the turbulent extreme wind model (10-min) for offshore turbine design (IEC, 2019b). These results suggest that the turbulent extreme wind model underestimates winds, especially near the tropical cyclone eyewall, for both Class I and Class T turbines.

Wind speed gusts near the eyewall are sometimes faster than expected in offshore design standards for category-2 and category-3 tropical cyclones (Figure 6a). Wind gusts exceed design specifications for the Class I turbine nearly 10% of the time in the category-3 storm. For the category-2 tropical cyclones, 3-sec winds exceed design specifications less than 5% of the time. Wind conditions in all storms rarely exceed 3-sec design criteria for Class T turbines for 50-year return periods. Worsnop, Lundquist, et al. (2017) also showed wind gusts in tropical cyclones can exceed design standards for Class I turbines for a category-5 storm. They report 3-sec winds can be 1.7 faster than 10-min winds near the eyewall (Worsnop, Lundquist, et al., 2017). For a limited number of hurricanes, Vickery and Skerlj (2005) also reports high wind gusts. They show 5-sec averaged winds can exceed 70 m s^{-1} when 10-min winds are at least 50 m s^{-1} at 40 m above the surface. Even though the steady extreme wind model (3-sec) is not recommended for offshore wind turbines, the IEC 61400–1 standard suggests this model for onshore wind turbine design (IEC, 2019a). These results suggest that the steady extreme wind model may underestimate winds for Class I turbines, especially near the eyewall of high-intensity tropical cyclones.

Wind speed shear in tropical cyclones is also larger than in the IEC extreme wind models (Figure 7). The mean power law exponent, α , in our simulations is calculated to have an average value around 0.2, nearly twice as large as the values specified for the turbulent and steady extreme wind models (i.e. $\alpha = 0.11$). Furthermore, as hub-height winds are faster than anticipated, wind speed in the upper rotor layer also exceeds design specifications. Note that the IEC standards include an extreme wind shear model with $\alpha = 0.2$ for use when turbines are in operation (DLC 1.1-1.5). This finding may suggest that an additional provision in the standards could be made to recommend the use of the extreme shear model exponent, $\alpha = 0.2$, for design load calculations during tropical cyclones as well.

Wind speed variability is also potentially underestimated for design load calculations. For the Class I (Class T) turbine for very high turbulence characteristics (i.e., A+ category), the normal turbulence model anticipates $\sigma_1 = 5.7 \text{ m s}^{-1}$ (6.4 m s^{-1}). The standard deviation of the horizontal velocity at the eyewall is on average 3, 4.5, and 5.7 m s^{-1} for the category-1, category-2 and category-3 storms, respectively. Nonetheless, extreme wind conditions in tropical cyclones can result in $\sigma_1 > 10 \text{ m s}^{-1}$ for at least 5% of cases for all storm categories. Therefore, design specifications for 50-year recurrence events could incorporate a larger standard deviation to represent the higher turbulence levels that can occur in tropical cyclones.

Wind direction shifts across the turbine rotor layer are also significant in tropical cyclones. Hub-height wind direction changes over short time periods (10-sec) typically do not exceed $\pm 20^\circ$ and only occasionally (17% probability of occurrence) exceed $\pm 8^\circ$ for the tropical cyclones simulated here (Figure 10). We do not expect extreme changes in hub-height wind direction throughout our simulations because the tropical cyclones are in a quasi-steady state. In reality, tropical cyclones drift over time, potentially resulting in $\pm 180^\circ$ changes in wind direction as the storm moves over the wind plant. Nevertheless, all storms evidence large wind veer across the turbine rotor layer (Figure 11). Current design specifications do not account for the increased loads from wind veer (Kapoor et al., 2020). We find wind veer does not change dramatically between storm intensities nor radial location. As a result, we expect the faster winds in the category-3 storm to

increase loads more compared to the category-1 storm. The influence from veer should be tested in load simulators to assess its importance on design standards for tropical cyclones of varying intensity levels.

These results can help improve design standards for offshore wind turbines in regions prone to tropical cyclones. Investigation of the actual loads induced by the wind gusts, turbulence levels, yaw misalignment and veer discussed here can provide guidance on the modifications required to build turbines for regions with high-risk of tropical cyclones. Note that the simulations presented here likely provide a conservative estimate of the extreme conditions occurring in the turbine rotor layer. Ren et al. (2020, 2022); Ito et al. (2017) show that turbulence statistics vary with increased grid resolution. As a result, wind gusts in the tropical cyclone eyewall can be faster and wind direction changes more severe, increasing loads on wind turbine support structures and blades. Refinements to the LES should also be explored to include wave effects, which are required for design load calculations in the IEC standards. Adding wind-wave coupling can provide additional information about the sea state in the tropical cyclone, which also influences loads on the support structure of offshore wind turbines (Kim et al., 2016).

Open Research Section

Data area available via <ftp://breeze.colorado.edu/pub/> using the *Guest* login. High-frequency output for each storm are stored in the OWIND directory.

Acknowledgments

We would like to acknowledge advice from Dr. Jimmy Dudhia and Dr. Hehe Ren on the simulation setup and spinup of the tropical cyclones.

This material is based upon work supported by the National Offshore Wind Research and Development Consortium. Any opinions, findings, and conclusions expressed in this material are those of the authors and do not necessarily reflect the views of the Consortium or other sponsors.

This work was authored (in part) by the National Renewable Energy Laboratory, operated by Alliance for Sustainable Energy, LLC, for the U.S. Department of Energy (DOE) under Contract No. DE-AC36-08GO28308. Funding provided by the U.S. Department of Energy Office of Energy Efficiency and Renewable Energy Wind Energy Technologies Office. The views expressed in the article do not necessarily represent the views of the DOE or the U.S. Government. The U.S. Government retains and the publisher, by accepting the article for publication, acknowledges that the U.S. Government retains a nonexclusive, paid-up, irrevocable, worldwide license to publish or reproduce the published form of this work, or allow others to do so, for U.S. Government purposes. The research was performed using computational resources sponsored by DOE and located at the National Renewable Energy Laboratory.

References

- Archer, C. L., Colle, B. A., Veron, D. L., Veron, F., & Sienkiewicz, M. J. (2016). On the predominance of unstable atmospheric conditions in the marine boundary layer offshore of the U.S. northeastern coast. *Journal of Geophysical Research: Atmospheres*, 121(15), 8869–8885. doi: 10.1002/2016JD024896
- Bardal, L. M., Sætran, L. R., & Wangsness, E. (2015). Performance test of a 3MW wind turbine – effects of shear and turbulence. *Energy Procedia*, 80, 83–91. doi: 10.1016/j.egypro.2015.11.410
- Bodini, N., Lundquist, J. K., & Kirincich, A. (2019). U.S. East Coast lidar

- measurements show offshore wind turbines will encounter very low atmospheric turbulence. *Geophysical Research Letters*, 46(10), 5582–5591. doi: 10.1029/2019GL082636
- Churchfield, M. J., & Srinivas, S. (2018). On the effects of wind turbine wake skew caused by wind veer. In *2018 wind energy symposium*. American Institute of Aeronautics and Astronautics. doi: 10.2514/6.2018-0755
- Donelan, M. A. (2004). On the limiting aerodynamic roughness of the ocean in very strong winds. *Geophysical Research Letters*, 31(18), L18306. doi: 10.1029/2004GL019460
- Dudhia, J., Done, J., Wang, W., Chen, Y., Xiao, Q., Davis, C., ... Torn, R. (2008). Prediction of atlantic tropical cyclones with the advanced hurricane WRF (AHW) model. In *28th conference on hurricanes and tropical meteorology*. American Meteorological Society.
- Franklin, J. L., Black, M. L., & Valde, K. (2003). GPS dropwindsonde wind profiles in hurricanes and their operational implications. *Weather and Forecasting*, 18(1), 32–44. doi: 10.1175/1520-0434(2003)018<0032:GDWPIH>2.0.CO;2
- Gao, L., Li, B., & Hong, J. (2021). Effect of wind veer on wind turbine power generation. *Physics of Fluids*, 33(1), 015101. doi: 10.1063/5.0033826
- Hallowell, S. T., Myers, A. T., Arwade, S. R., Pang, W., Rawal, P., Hines, E. M., ... Fontana, C. M. (2018). Hurricane risk assessment of offshore wind turbines. *Renewable Energy*, 125, 234–249. doi: 10.1016/j.renene.2018.02.090
- Hock, T. F., & Franklin, J. L. (1999). The NCAR GPS dropwindsonde. *Bulletin of the American Meteorological Society*, 80(3), 407–420. doi: 10.1175/1520-0477(1999)080<0407:TNGD>2.0.CO;2
- Hong, S., & Lim, J. (2006). The WRF single-moment 6-class microphysics scheme (WSM6). *Asia-pacific Journal of Atmospheric Sciences*, 42, 129–151.
- Hong, S.-Y., Noh, Y., & Dudhia, J. (2006). A new vertical diffusion package with an explicit treatment of entrainment processes. *Monthly Weather Review*, 134(9), 2318–2341. doi: 10.1175/MWR3199.1
- IEC. (2019a). *Wind turbines - part 1: Design requirements* (No. IEC 61400-1:2019).
- IEC. (2019b). *Wind turbines - part 3: Design requirements for offshore wind turbines* (No. IEC 61400-3-1:2019).
- Ito, J., Oizumi, T., & Niino, H. (2017). Near-surface coherent structures explored by large eddy simulation of entire tropical cyclones. *Scientific Reports*, 7(1), 3798. doi: 10.1038/s41598-017-03848-w
- Jiménez, P. A., Dudhia, J., González-Rouco, J. F., Navarro, J., Montávez, J. P., & García-Bustamante, E. (2012). A revised scheme for the WRF surface layer formulation. *Monthly Weather Review*, 140(3), 898–918. doi: 10.1175/MWR-D-11-00056.1
- Jonkman, J., Butterfield, S., Musial, W., & Scott, G. (2009). *Definition of a 5-MW reference wind turbine for offshore system development* (No. NREL/TP-500-38060).
- Jordan, C. L. (1958). Mean soundings for the west indies area. *Journal of Meteorology*, 15(1), 91–97. doi: 10.1175/1520-0469(1958)015<0091:MSFTWI>2.0.CO;2
- Kaimal, J. C., Wyngaard, J. C., Izumi, Y., & Coté, O. R. (1972). Spectral characteristics of surface-layer turbulence. *Quarterly Journal of the Royal Meteorological Society*, 98(417), 563–589. doi: 10.1002/qj.49709841707
- Kapoor, A., Ouakka, S., Arwade, S. R., Lundquist, J. K., Lackner, M. A., Myers, A. T., ... Bryan, G. H. (2020). Hurricane eyewall winds and structural response of wind turbines. *Wind Energy Science*, 5(1), 89–104. doi: 10.5194/wes-5-89-2020
- Keim, B. D., Muller, R. A., & Stone, G. W. (2007). Spatiotemporal patterns and return periods of tropical storm and hurricane strikes from Texas to Maine. *Journal of Climate*, 20(14), 3498–3509. doi: 10.1175/JCLI4187.1
- Kim, E., Manuel, L., Curcic, M., Chen, S. S., Phillips, C., & Veers, P. (2016). On

- the use of coupled wind, wave, and current fields in the simulation of loads on bottom-supported offshore wind turbines during hurricanes (No. NREL/TP-5000-65283).
- Kosović, B. (1997). Subgrid-scale modelling for the large-eddy simulation of high-Reynolds-number boundary layers. *Journal of Fluid Mechanics*, 336, 151–182. doi: 10.1017/S0022112096004697
- Li, X., Pu, Z., & Gao, Z. (2021). Effects of roll vortices on the evolution of hurricane Harvey during landfall. *Journal of the Atmospheric Sciences*, 78(6), 1847–1867. doi: 10.1175/JAS-D-20-0270.1
- Mann, J. (1994). The spatial structure of neutral atmospheric surface-layer turbulence. *Journal of Fluid Mechanics*, 273, 141–168. doi: 10.1017/S0022112094001886
- Marks, F. D., & Houze, R. A. (1984). Airborne doppler radar observations in hurricane Debby. *Bulletin of the American Meteorological Society*, 65(6), 569–582. doi: 10.1175/1520-0477(1984)065<0569:ADROIH>2.0.CO;2
- Mazzaro, L. J., Muñoz-Esparza, D., Lundquist, J. K., & Linn, R. R. (2017). Nested mesoscale-to-LES modeling of the atmospheric boundary layer in the presence of under-resolved convective structures. *Journal of Advances in Modeling Earth Systems*, 9(4), 1795–1810. doi: 10.1002/2017MS000912
- Mirocha, J. D., Lundquist, J. K., & Kosović, B. (2010). Implementation of a nonlinear subfilter turbulence stress model for large-eddy simulation in the advanced research WRF model. *Monthly Weather Review*, 138(11), 4212–4228. doi: 10.1175/2010MWR3286.1
- Moeng, C.-H., Dudhia, J., Klemp, J., & Sullivan, P. (2007). Examining two-way grid nesting for large eddy simulation of the PBL using the WRF model. *Monthly Weather Review*, 135(6), 2295–2311. doi: 10.1175/MWR3406.1
- Musial, W., Spitsen, P., Duffy, P., Beiter, P., Marquis, M., Hammond, R., & Shields, M. (2022). *Offshore wind market report: 2022 edition*.
- Muñoz-Esparza, D., Lundquist, J. K., Sauer, J. A., Kosović, B., & Linn, R. R. (2017). Coupled mesoscale-LES modeling of a diurnal cycle during the CWEX -13 field campaign: From weather to boundary-layer eddies. *Journal of Advances in Modeling Earth Systems*, 9(3), 1572–1594. doi: 10.1002/2017MS000960
- National Hurricane Center. (2021). *The Saffir-Simpson hurricane wind scale*.
- Neumann, C. (2010). *The national hurricane center risk analysis program (HURISK)* [NWS NHC 38].
- Nolan, D. S., Zhang, J. A., & Uhlhorn, E. W. (2014). On the limits of estimating the maximum wind speeds in hurricanes. *Monthly Weather Review*, 142(8), 2814–2837. doi: 10.1175/MWR-D-13-00337.1
- Ren, H., Dudhia, J., Ke, S., & Li, H. (2022). The basic wind characteristics of idealized hurricanes of different intensity levels. *Journal of Wind Engineering and Industrial Aerodynamics*, 225, 104980. doi: 10.1016/j.jweia.2022.104980
- Ren, H., Dudhia, J., & Li, H. (2020). Large-eddy simulation of idealized hurricanes at different sea surface temperatures. *Journal of Advances in Modeling Earth Systems*, 12(9). doi: 10.1029/2020MS002057
- Robertson, A. N., Shaler, K., Sethuraman, L., & Jonkman, J. (2019). Sensitivity analysis of the effect of wind characteristics and turbine properties on wind turbine loads. *Wind Energy Science*, 4(3), 479–513. doi: 10.5194/wes-4-479-2019
- Rotunno, R., Chen, Y., Wang, W., Davis, C., Dudhia, J., & Holland, G. J. (2009). Large-eddy simulation of an idealized tropical cyclone. *Bulletin of the American Meteorological Society*, 90(12), 1783–1788. doi: 10.1175/2009BAMS2884.1
- Rotunno, R., & Emanuel, K. A. (1987). An air-sea interaction theory for tropical cyclones. part II: Evolutionary study using a nonhydrostatic axisymmetric

- numerical model. *Journal of the Atmospheric Sciences*, 44(3), 542–561. doi: 10.1175/1520-0469(1987)044<0542:AAITFT>2.0.CO;2
- Sanchez Gomez, M., & Lundquist, J. K. (2020). The effect of wind direction shear on turbine performance in a wind farm in central Iowa. *Wind Energy Science*, 5(1), 125–139. doi: 10.5194/wes-5-125-2020
- Skamarock, W. C. (2004). Evaluating mesoscale NWP models using kinetic energy spectra. *Monthly Weather Review*, 132(12), 3019–3032. doi: 10.1175/MWR2830.1
- Skamarock, W. C., Klemp, J. B., Dudhia, J., Gill, D. O., Liu, Z., Berner, J., . . . Huang, X.-Y. (2019). *A description of the advanced research WRF model version 4*. doi: 10.5065/1DFH-6P97
- Stern, D. P., Bryan, G. H., Lee, C.-Y., & Doyle, J. D. (2021). Estimating the risk of extreme wind gusts in tropical cyclones using idealized large-eddy simulations and a statistical–dynamical model. *Monthly Weather Review*, 149(12), 4183–4204. doi: 10.1175/MWR-D-21-0059.1
- The White House. (2022). *FACT SHEET: Biden-Harris Administration Announces New Actions to Expand U.S. Offshore Wind Energy*. (Accessed on April 8, 2023)
- Vanderwende, B. J., Lundquist, J. K., Rhodes, M. E., Takle, E. S., & Irvin, S. L. (2015). Observing and simulating the summertime low-level jet in central Iowa. *Monthly Weather Review*, 143(6), 2319–2336. doi: 10.1175/MWR-D-14-00325.1
- Vickery, P. J., & Skerlj, P. F. (2005). Hurricane gust factors revisited. *Journal of Structural Engineering*, 131(5), 825–832. doi: 10.1061/(ASCE)0733-9445(2005)131:5(825)
- Worsnop, R. P., Bryan, G. H., Lundquist, J. K., & Zhang, J. A. (2017). Using large-eddy simulations to define spectral and coherence characteristics of the hurricane boundary layer for wind-energy applications. *Boundary-Layer Meteorology*, 165(1), 55–86. doi: 10.1007/s10546-017-0266-x
- Worsnop, R. P., Lundquist, J. K., Bryan, G. H., Damiani, R., & Musial, W. (2017). Gusts and shear within hurricane eyewalls can exceed offshore wind turbine design standards. *Geophysical Research Letters*, 44(12), 6413–6420. doi: 10.1002/2017GL073537
- Wurman, J., & Kosiba, K. (2018). The role of small-scale vortices in enhancing surface winds and damage in hurricane Harvey (2017). *Monthly Weather Review*, 146(3), 713–722. doi: 10.1175/MWR-D-17-0327.1
- Wurman, J., & Winslow, J. (1998). Intense sub-kilometer-scale boundary layer rolls observed in hurricane Fran. *Science*, 280(5363), 555–557. doi: 10.1126/science.280.5363.555
- Wyngaard, J. C. (2004). Toward numerical modeling in the “terra incognita”. *Journal of the Atmospheric Sciences*, 61(14), 1816–1826. doi: 10.1175/1520-0469(2004)061<1816:TNMITT>2.0.CO;2